

Development of a quantitative method for the characterization of hole quality during laser trepan drilling of high-temperature alloy

Hongyu Zhang¹ · Ming Zhou¹ · Yunlong Wang² · Xiangchao Zhang³ · Yu Yan⁴ · Rong Wang¹

Received: 9 September 2015 / Accepted: 3 January 2016 / Published online: 22 January 2016
© Springer-Verlag Berlin Heidelberg 2016

Abstract Short-pulsed lasers are of significant industrial relevance in laser drilling, with an acceptable compromise between accuracy and efficiency. However, an intensive research with regard to qualitative and quantitative characterization of the hole quality has rarely been reported. In the present study, a series of through holes were fabricated on a high-temperature alloy workpiece with a thickness of 3 mm using a LASERTEC 80 PowerDrill manufacturing system, which incorporated a Nd:YAG millisecond laser into a five-axis positioning platform. The quality of the holes manufactured under different laser powers (80–140 W) and beam expanding ratios (1–6) was characterized by a scanning electron microscope associated with an energy-dispersive X-ray analysis, focusing mainly on the formation of micro-crack and recast layer. Additionally, the conicity and circularity of the holes were quantitatively evaluated by the apparent radius, root-mean-square deviation, and maximum deviation, which were calculated based on the extraction of hole edge through

programming with MATLAB. The results showed that an amount of melting and spattering contents were presented at the entrance end and the exit end of the holes, and micro-cracks and recast layer (average thickness 15–30 μm) were detected along the side wall of the holes. The elemental composition of the melting and spattering contents and the recast layer was similar, with an obvious increase in the contents of O, Nb, and Cr and a great reduction in the contents of Fe and Ni in comparison with the bulk material. Furthermore, the conicity and circularity evaluation of the holes indicated that a laser power of 100 W and a beam expanding ratio of 4 or 5 represented the typical optimal drilling parameters in this specific experimental situation. It is anticipated that the quantitative method developed in the present study can be applied for the evaluation of hole quality in laser drilling and other drilling conditions.

1 Introduction

Nowadays, laser manufacturing has been adopted as an effective technology to produce micro-features in various materials, such as metal, silicon, and ceramic [1]. As an intensified thermal source, the focused laser beam can achieve removal of materials according to a predetermined path through melting or vaporization [2]. The great demand for precision holes has promoted rapid development of laser drilling in many fields. Specifically, laser drilling has been applied in aerospace industry to manufacture shaped film holes in turbine blade. These film holes vary significantly in morphology and inclination angle, forming a protective cooling layer between the hot gases and the external surfaces of the turbine blade [3]. Generally, three strategies have been developed to fulfill different requirements in laser drilling, including single pulse drilling,

✉ Ming Zhou
zhouming@tsinghua.edu.cn

Hongyu Zhang
zhanghyu@tsinghua.edu.cn

- ¹ State Key Laboratory of Tribology, Department of Mechanical Engineering, Tsinghua University, Beijing 100084, China
- ² School of Material Science and Engineering, Jiangsu University, Zhenjiang 212013, China
- ³ Shanghai Engineering Research Centre of Ultra-Precision Optical Manufacturing, Fudan University, Shanghai 200438, China
- ⁴ Corrosion and Protection Center, Beijing University of Science and Technology, Beijing 100083, China

percussion drilling, and trepan drilling [4, 5]. However, regardless of the use of either drilling strategy, the molten material tends to re-solidify on the side wall of the holes and results in the formation of a so-called recast layer, which is extremely detrimental due to the introduction of potential sites with an amount of micro-cracks [6, 7].

Over the years, different attempts have been tried to reduce the thickness of recast layer and to improve the quality (e.g., morphology, circularity, conicity) of holes prepared by laser drilling, including ultrasonic vibration [8], water jet-guided fabrication [9], and helical drilling strategy [10]. Alternatively, ultrafast laser, represented typically by picosecond and femtosecond lasers, has been advocated for the manufacturing of precision holes because the materials are mainly removed through vaporization and almost no thermal effects occur during this process [11, 12]. For example, picosecond laser helical drilling, associated with a high-speed laser beam rotation apparatus, has been reported to manufacture various holes on stainless steel with very high quality (recast layer thickness less than 5 μm) in comparison with nanosecond laser drilling [13, 14]. However, conventional short-pulsed lasers still play an important role in laser drilling as a result of the enhanced drilling efficiency on condition that the drilling parameters are optimally adjusted [15]. From a systematic review of previous studies, it is realized that the characterizations of hole quality are generally morphology based and an intensive examination containing both qualitative and quantitative descriptions has not been available. Therefore, in the present study, we primarily aim to develop a method for quantitative evaluation of the quality of holes during laser drilling.

2 Materials and methods

2.1 Experimental setup

A series of laser drilling experiments were performed on a high-temperature alloy workpiece (GH169 in China, also known as Inconel 718 internationally, thickness 3.0 mm) employing a LASERTEC 80 PowerDrill manufacturing system (DMG Asia Pacific Pte Ltd, Singapore), which incorporated a Nd:YAG laser (wave length 1064 nm; pulse length 0.1–20 ms; pulse frequency 0.1–500 Hz; maximum power 300 W) into a five-axis positioning platform ($X/Y/Z$ axis range 800 mm \times 500 mm \times 700 mm; $X/Y/Z$ axis accuracy 0.01 mm; swivel/rotary axis range -90° – 160° / 360°). The laser beam travelled within the drilling head (along Z axis) and passed through the nozzle before reaching the workpiece, and the assist gas was supplied coaxially through the nozzle, blowing away the molten materials during drilling process. The workpiece was polished

consecutively using abrasive paper (280[#], 600[#], 1000[#], and 2000[#]) and polyurethane polishing pad with the presence of diamond paste (size 1.5 μm). The surface roughness value was measured by a micro-XAM-3D optical interferometer (~ 30 nm), with a scanning area of 0.8×0.6 mm².

The trepan strategy was adopted to drill through holes (diameter 0.5 mm) on the workpiece, which was achieved by precise movement of the positioning platform (with the workpiece stably attached) in the horizontal plane. The primary drilling parameters were summarized under two experimental conditions as follows: (1) laser power 80–140 W; beam expanding ratio 4; and assist oxygen pressure 0.4 MPa and (2) laser power 100 W; beam expanding ratio 1–6; and assist oxygen pressure 0.4 MPa. All the holes were drilled vertically at 90° to the workpiece, with the laser beam focusing on the top surface by a focusing lens (focal distance 150 mm; focus diameter ~ 0.2 mm). Note that focus diameter is affected by beam expansion and laser power, and it varies under different setup). The other drilling conditions were summarized as follows: (a) pulse duration 1 ms; (b) laser repetition rate 30 Hz; (c) trepanning path diameter 0.5 mm; (d) trepanning velocity 25 mm/min; (e) repetition of the trepanning path 5 loops. The separation of every two holes was at least 5 mm, in order to avoid the thermal effects during laser trepan drilling. The fabrication of each hole was repeated three times to enable statistical validity.

2.2 Characterization of hole quality

2.2.1 Morphological and elemental analyses

Following completion of laser trepan drilling, the entrance end and the exit end of the holes were examined using a Quanta 200 FEG scanning electron microscope (SEM, FEI, Eindhoven, Netherlands) to detect the formation of melting and spattering contents surrounding the holes, without any treatment of the workpiece. Additionally, a comparison of elemental composition between the bulk material and the melting and spattering contents was performed employing an energy-dispersive X-ray (EDX) analysis.

2.2.2 Apparent radius, RMS deviation, and maximum deviation

The boundary of the holes at both the entrance end and the exit end was matched on the SEM micrographs through programming with MATLAB 7, based on the extraction of the gradient level. In detail, the boundary of one hole was considered to be composed of points with the greatest gradient. Therefore, the edge points were determined by $\Omega = \{p(x, y) \mid |\nabla p(x, y)| > \delta\}$, where δ was an adaptive threshold obtained from the measured surface. Note that

due to the presence of potential defects on the surface, some false points may be taken as edge points inappropriately. In this case, the morphological operators such as dilation and erosion can be used to eliminate isolated defects [16]. Subsequently, the edge curve of the hole was fitted as a circle using the least-squares method $(a, b, r) = \arg \min_{p(x,y) \in \Omega} \left[r - \sqrt{(x-a)^2 + (y-b)^2} \right]^2$, and the apparent radius r was determined. The average value of the apparent radius was obtained for the holes fabricated with the same drilling parameters, and the conicity of the holes was calculated as the value of the apparent radius of the entrance end divided by that of the exit end. Additionally, the average values of the RMS deviation and the maximum deviation (nominated as the root-mean-squares value and the peak-to-valley value of the difference between the edge curve of the hole and the fitted circle, respectively) were also calculated to evaluate circularity of the holes quantitatively.

2.2.3 Micro-cracks and recast layer

The workpiece was slightly polished employing polyurethane polishing pad with the presence of diamond paste

(size 1.5 μm) to remove the melting and spattering contents on the surface and investigated using the SEM at an inclined angle of 20°, through which the formation of potential micro-cracks along the side wall of the holes could be observed. Subsequently, the workpiece was fabricated into smaller fragments through wire electrode cutting (with one hole on each fragment), and all the fragments were mounted stably within an EpoFix resin (Struers, Denmark) after curing overnight. Finally, the longitudinal section of the holes was adequately polished, exposed, and investigated using the SEM associated with EDX analysis to enable the examination of recast layer along the side wall of the holes and the comparison of elemental composition between the bulk material and the recast layer.

3 Results

3.1 Evaluation of morphology and element by SEM and EDX

The SEM micrographs shown in Figs. 1 and 2 demonstrated the surface morphology of the entrance end and the exit end of the through holes fabricated on the high-

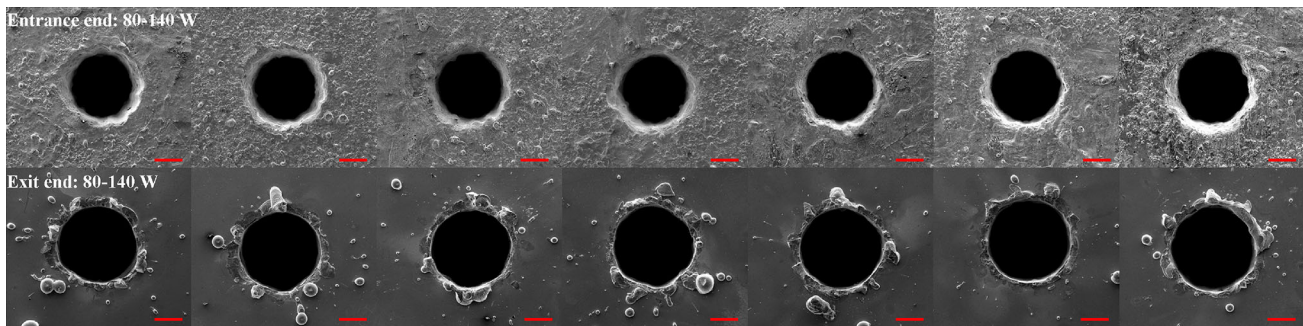


Fig. 1 SEM micrographs showing surface morphology of the entrance end and the exit end of the holes, with different laser powers from 80 to 140 W. Bar 0.2 mm

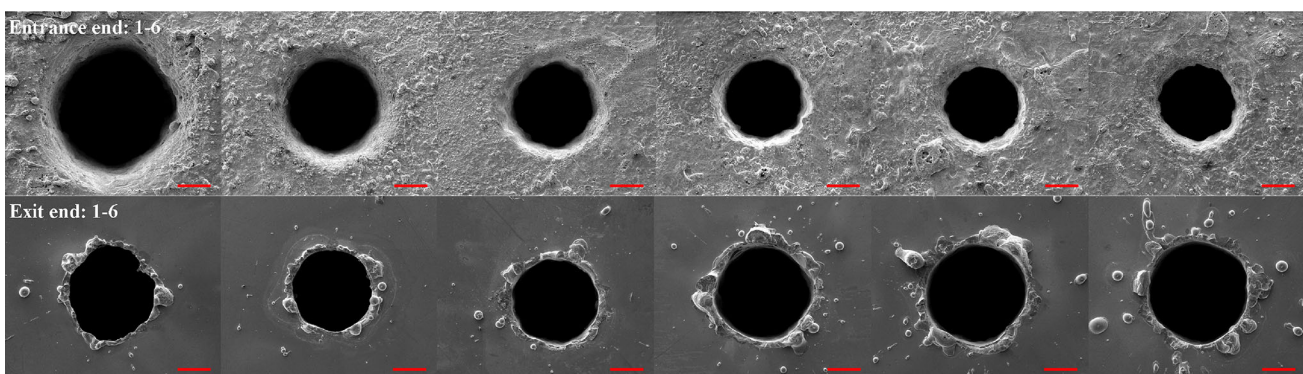


Fig. 2 SEM micrographs showing surface morphology of the entrance end and the exit end of the holes, with different beam expanding ratios from 1 to 6. Bar 0.2 mm

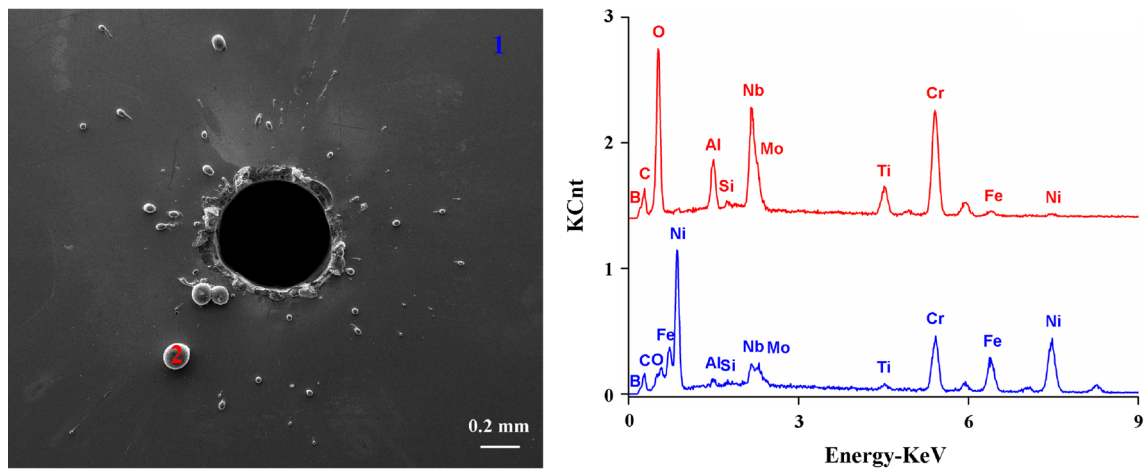


Fig. 3 Comparison of elemental composition between the bulk material (Area 1) and the melting and spattering contents (Area 2) of high-temperature alloy. Laser power 80 W; beam expanding ratio 4

Table 1 Comparison of elemental composition (wt%) between the bulk material and the melting and spattering contents of high-temperature alloy

Element	B	C	O	Al	Si	Nb	Mo	Ti	Cr	Fe	Ni
Bulk material 1	2.15	4.95	0.25	0.79	0.27	5.10	2.67	1.19	17.61	16.88	48.14
Melting and spattering contents 2	2.95	5.50	22.65	3.70	0.36	19.15	0.57	5.84	34.67	2.47	2.15

temperature alloy workpiece with different laser powers (80–140 W) and beam expanding ratios (1–6). It was obvious that the entrance end appeared much rougher in comparison with the original workpiece, with the presence of a layer of melting and spattering contents which accumulated around the holes. The exit end was relatively smoother than the entrance end, and an amount of round-shaped melting and spattering contents were detected on the surface. It was indicated from a visual inspection of the SEM micrographs that the size of the holes manufactured with different laser powers was similar. However, with regard to those holes drilled with different beam expanding ratios, basically the size showed a decreasing trend at the entrance end and an increasing tendency at the exit end.

The comparison of elemental composition between the bulk material (Area 1) and the melting and spattering contents (Area 2) surrounding a hole (laser power 80 W; beam expanding ratio 4) is presented in Fig. 3 and Table 1. A significant increase in the contents of O, Nb, and Cr was observed, with an obvious reduction in the contents of Fe and Ni.

3.2 Characterization of apparent radius, RMS deviation, and maximum deviation

A typical example showing the fitting of hole edge on the SEM micrograph, represented by a white curve, is

demonstrated in Fig. 4. The calculation of apparent radius, RMS deviation, and maximum deviation at both the entrance end and the exit end of the holes fabricated with different laser powers (80–140 W) and beam expanding ratios (1–6) is displayed in Figs. 5 and 6, respectively.

As for the holes drilled with various laser powers, the apparent radius did not change markedly at the entrance end and the exit end. This was consistent with the visual observation from the SEM micrographs. However, it was noted that all the apparent radius values were larger than the pre-established input (diameter 0.5 mm). The conicity of the holes was calculated as 1.08, 1.06, 1.10, 1.07, 1.07, 1.06, and 1.10 for laser powers of 80–140 W, respectively. Additionally, the values of RMS deviation and maximum deviation varied greatly for different laser powers, and no obvious patterns were obtained. However, it seemed that a laser power of 100 W could represent a compromise choice with acceptable conicity and circularity.

Regarding the holes fabricated with different beam expanding ratios, the apparent radius decreased significantly at the entrance end with the increase in beam expanding ratio, while it displayed a slightly increasing trend at the exit end. Similarly, the apparent radius values were all larger than the pre-established input (diameter 0.5 mm). The conicity of the holes was 1.85, 1.56, 1.28, 1.10, 0.99, and 1.00 for beam expanding ratios of 1–6, respectively. In addition, the values of RMS deviation and

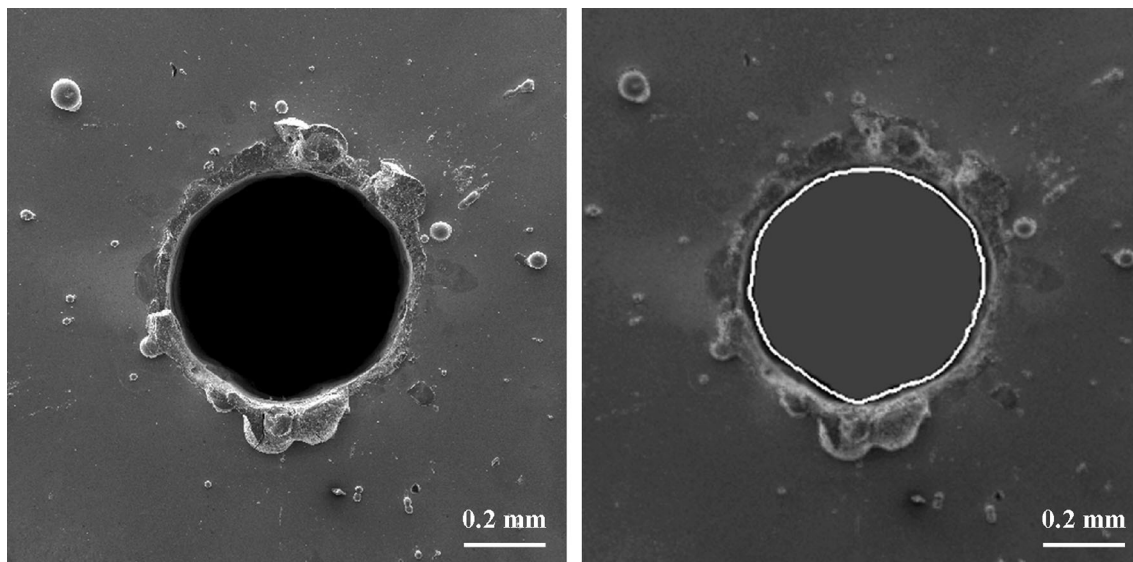


Fig. 4 A typical example demonstrating the fitting of hole edge on the SEM micrograph by programming with MATLAB 7

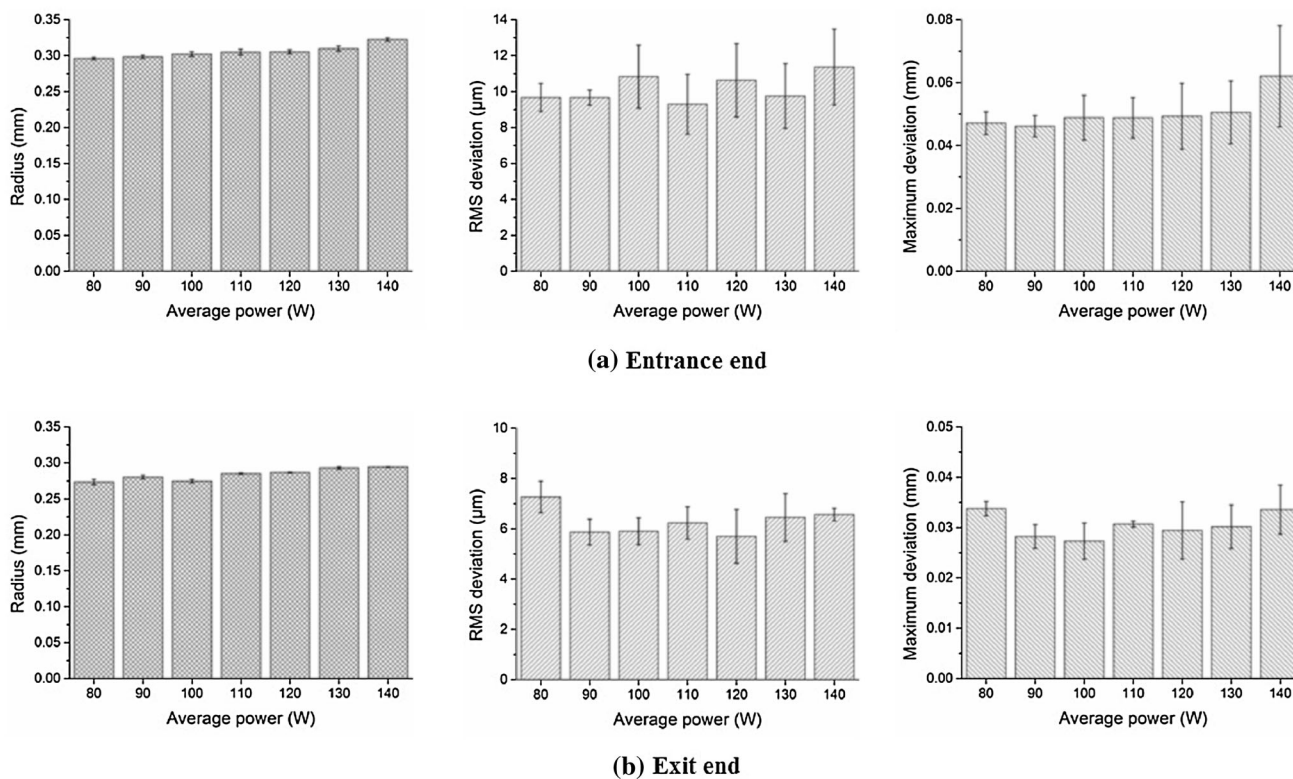


Fig. 5 Calculation of apparent radius, RMS deviation, and maximum deviation at the entrance end and the exit end of the holes, with different laser powers from 80 to 140 W

maximum deviation were relatively smaller for beam expanding ratios of 2, 4, and 5, indicating a good circularity of the holes. On the consideration of a larger conicity for the holes fabricated at beam expanding ratio of 2, it was considered that a beam expanding ratio of 4 or 5 was preferable.

3.3 Formation of micro-cracks and recast layer along the side wall of the holes

The side wall of the holes drilled with different laser powers (80–140 W) and beam expanding ratios (1–6) appeared very rough, and the formation of micro-cracks

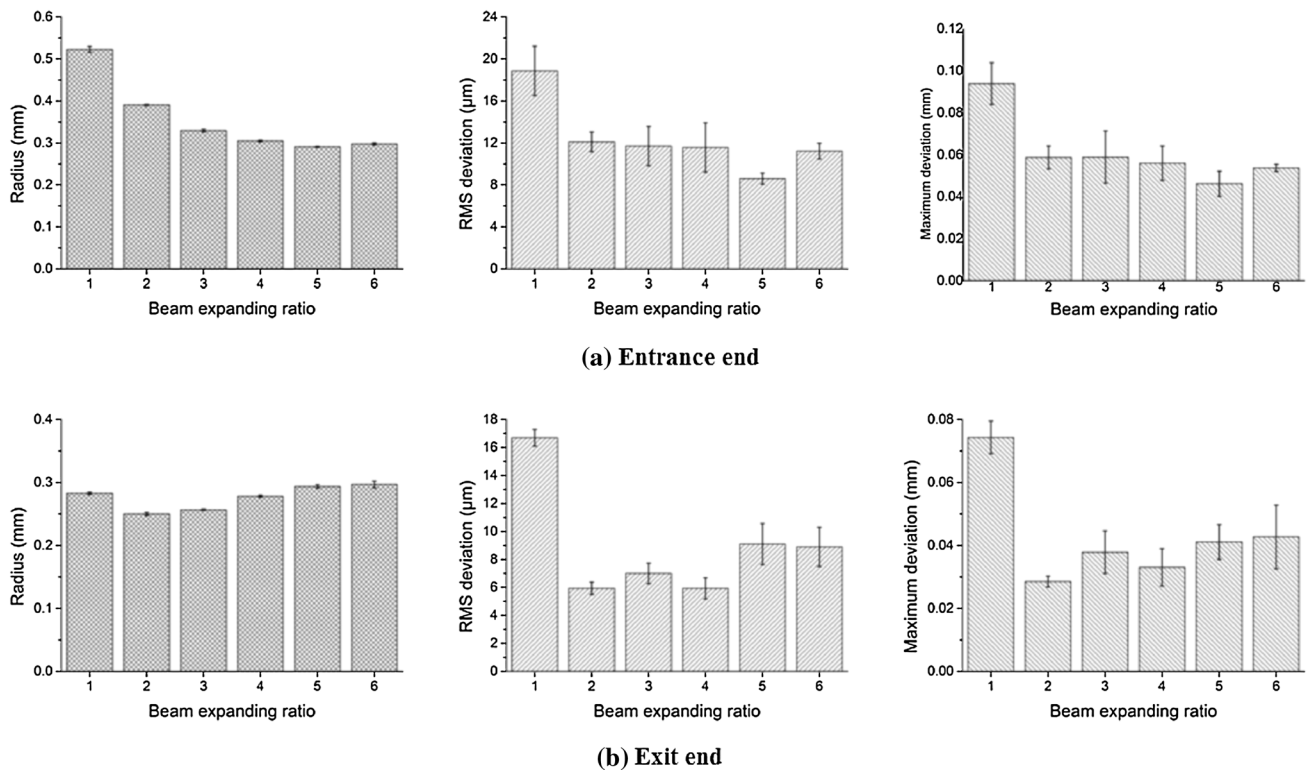


Fig. 6 Calculation of apparent radius, RMS deviation, and maximum deviation at the entrance end and the exit end of the holes, with different beam expanding ratios from 1 to 6

was clearly presented in two representative SEM micrographs with high magnification, as shown in Fig. 7a, b. The drilling parameters were as follows: (a) laser power 130 W; beam expanding ratio 4; (b) laser power 100 W; and beam expanding ratio 2.

Figures 8 and 9 demonstrate the longitudinal section of the holes fabricated with different laser powers (80–140 W) and beam expanding ratios (1–6), respectively. Regarding the holes drilled with various laser powers, it was indicated that the size of the holes was generally uniform from the entrance end to the exit end, especially for the laser powers of 100–140 W, Fig. 8a. The formation of recast layer along the side wall of a typical hole (laser power 80 W) is shown in Fig. 8b, and the average thickness of the recast layer was calculated to be about 15–30 μm . Additionally, the presence of micro-cracks within the recast layer was also observed, extending till the boundary of the bulk material. As for the holes manufactured with various beam expanding ratios, an obvious conicity was detected for the beam expanding ratios of 1–3, and the size of the holes was basically uniform for the beam expanding ratios of 4–6, Fig. 9a. Similarly, recast layer was presented along the side wall of the holes, and a typical example (beam expanding ratio 5) is demonstrated in Fig. 9b, with an average thickness of approximately 10–20 μm . Additionally, an amount of

micro-cracks were detected within the recast layer as well.

The comparison of elemental composition between the bulk material (Area 1) and the recast layer (Area 2) along the side wall of a hole (laser power 80 W; beam expanding ratio 4) is displayed in Fig. 10 and Table 2. It was clear that a significant increase in the contents of O, Nb, and Cr was observed, with a great reduction in the contents of Fe and Ni.

4 Discussion

The versatile ability of lasers to manufacture various holes with irregular shape and inclined direction has greatly promoted its application in aerospace, automotive, and medical industries. [17]. Nowadays, laser drilling has been accepted as a major technology for the manufacturing of the numerous shaped film holes located in the turbine blade, where short-pulsed lasers are mainly utilized based on the consideration of accuracy and efficiency. The removal of materials by short-pulsed lasers is dominated by heat conduction, and the molten contents will re-solidify and accumulate on the side wall of the holes, forming a recast layer, if they are not expelled rapidly and completely [18, 19]. Therefore, many researchers focus on the

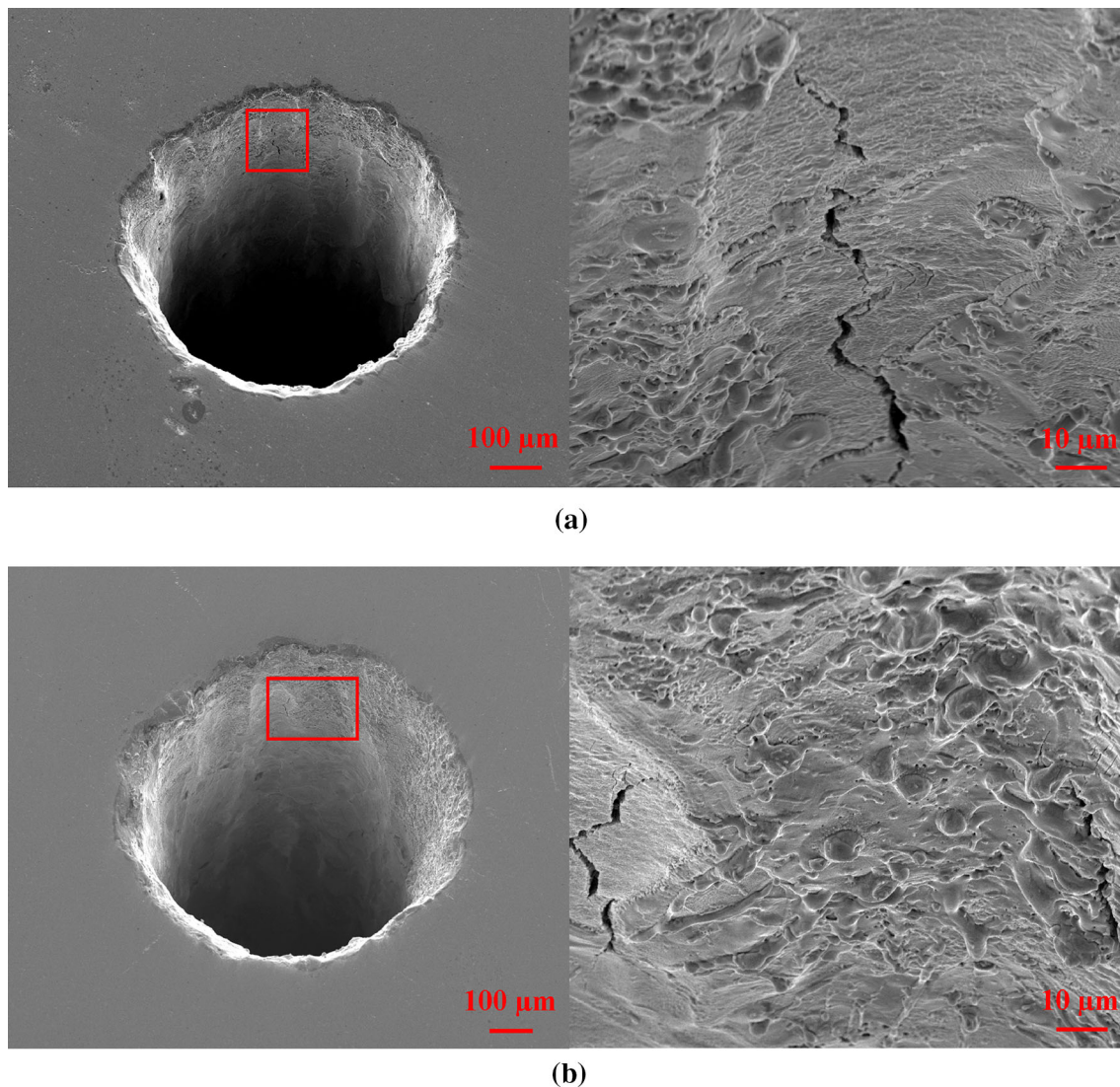


Fig. 7 Formation of micro-cracks along the side wall of the holes manufactured under different drilling conditions: **a** laser power 130 W; beam expanding ratio 4; **b** laser power 100 W; beam expanding ratio 2

development of optimal drilling parameters with short-pulsed lasers in order to improve laser drilling quality [20, 21].

In the present study, we performed a series of experiments on a high-temperature alloy using a Nd:YAG millisecond laser under trepan drilling strategy. The influence of two drilling parameters, i.e., laser power and beam expanding ratio, on the quality of the through holes was investigated based on both qualitative (SEM) and quantitative (EDX and MATLAB programming) characterizations. It was demonstrated that an amount of melting and spattering contents were observed at the entrance end and the exit end, with the presence of micro-cracks and a recast layer along the side wall of the holes. It was further confirmed by the comparison of elemental composition between the bulk material and the melting and spattering

content and between the bulk material and the recast layer, where an obvious increase in the content of O was obtained. This is considered to be attributed to the material removal process of short-pulsed laser drilling during which the molten contents are oxidized before they cool and re-solidify on the side wall of the holes, especially when oxygen is used as the assist gas. In addition, an assumption of the increase in the contents of Nb and Cr is considered to be related to the cooling process. As primary strengthening elements, Nb and Cr tend to precipitate under a relatively slow cooling process (air cooling in the present study), resulting in an obvious increase in the contents of these two elements. This, as a consequence, accounts for the decrease in the contents of Fe and Ni. The trepan strategy is an important factor to result in the formation of melting and spattering content and recast layer in the present study,

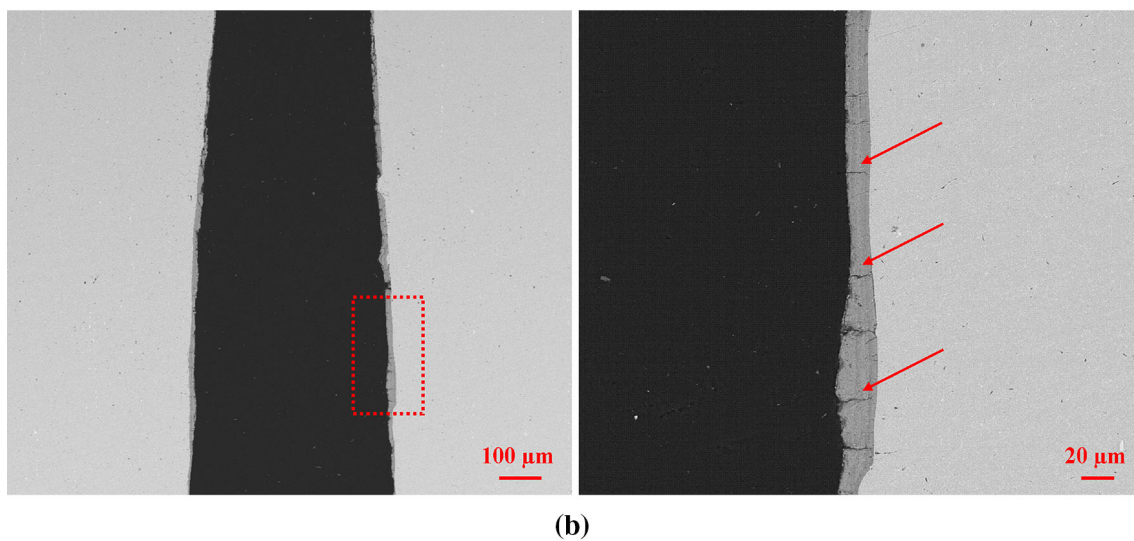
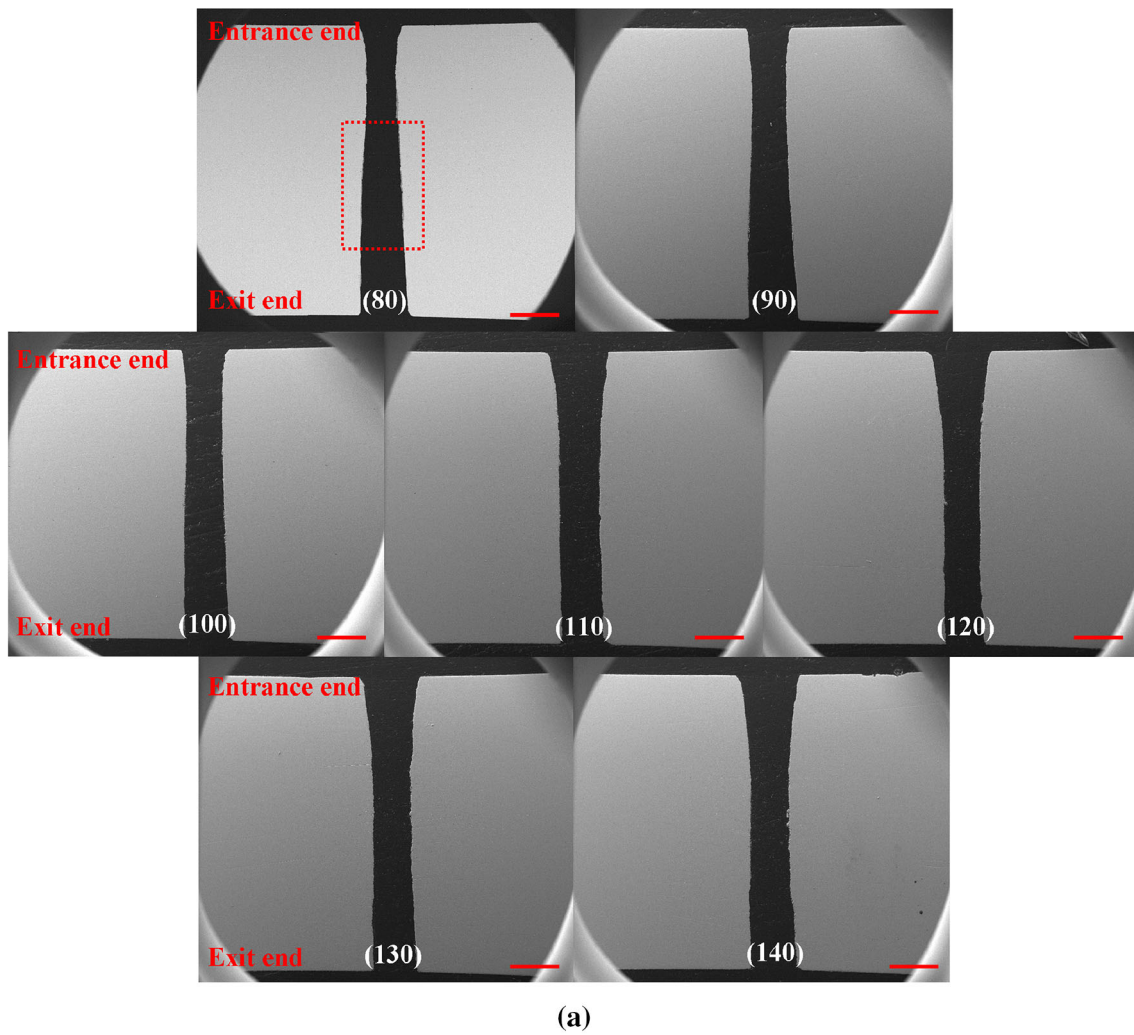


Fig. 8 **a** Longitudinal section of the holes drilled with different laser powers and **b** the formation of recast layer along the side wall (laser power 80 W, thickness 15–30 μm). Bar 0.5 mm. The *arrows* indicated the presence of micro-cracks within the recast layer

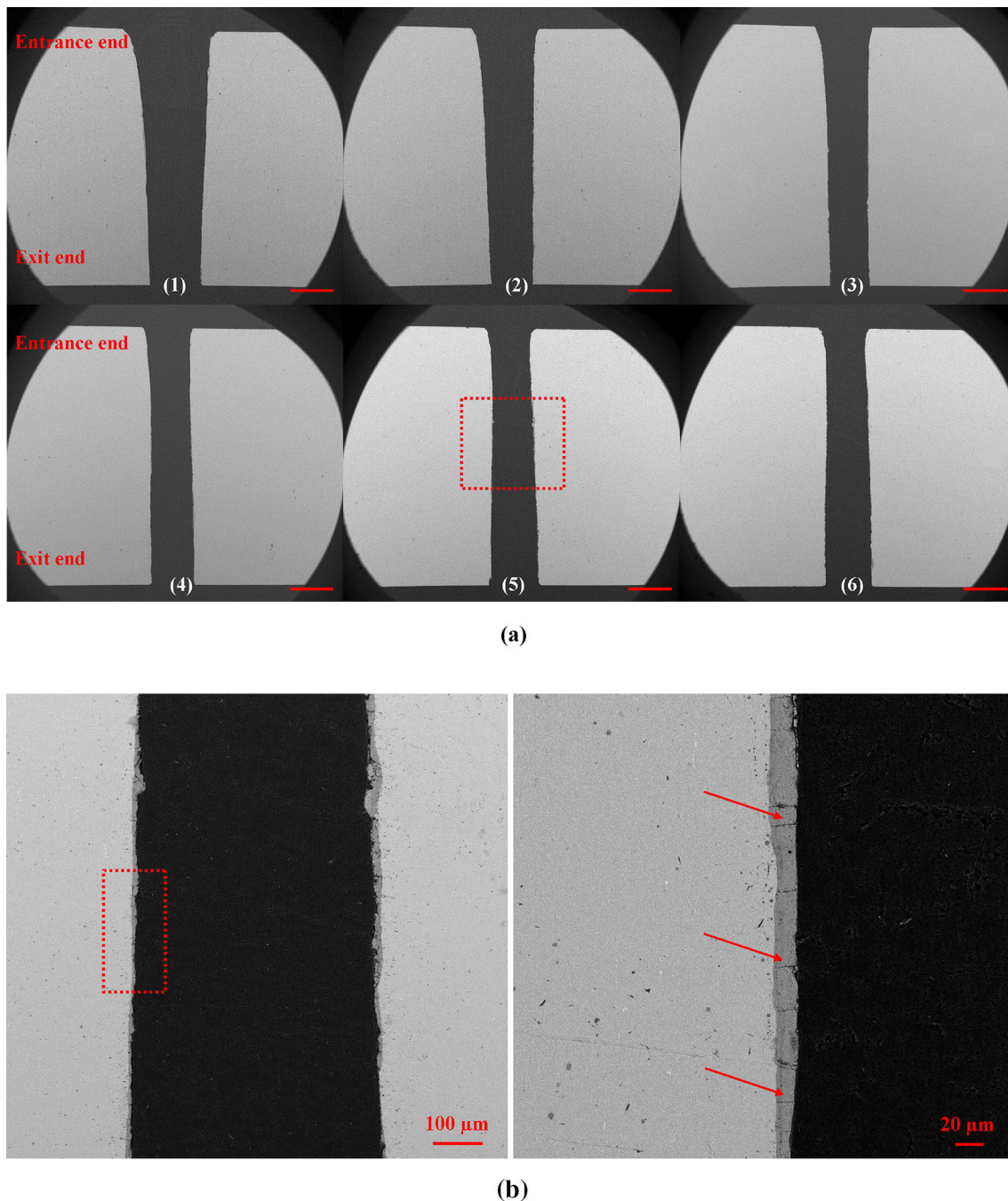


Fig. 9 **a** Longitudinal section of the holes drilled with different beam expanding ratios and **b** the formation of recast layer along the side wall (beam expanding ratio 5, thickness 10–20 μm). Bar 0.5 mm. The *arrows* indicated the presence of micro-cracks within the recast layer

because the materials are expelled axially along the side wall of the holes to the entrance end and cannot be removed laterally [22]. The valuable contribution of the present study is the development of a quantitative method for the calculation of conicity and circularity of the holes (represented by the apparent radius, RMS deviation, and maximum deviation), which can display the hole edge based on the extraction of gradient level of the SEM

micrograph. This quantitative method has potential application for the characterization of hole quality in other drilling conditions.

A limitation of the present study is that the preferable laser drilling parameters obtained based on the quantitative characterization of hole quality (laser power 100 W; beam expanding ratio 4 or 5) cannot be generalized because laser drilling is largely material-dependent. Additionally, only

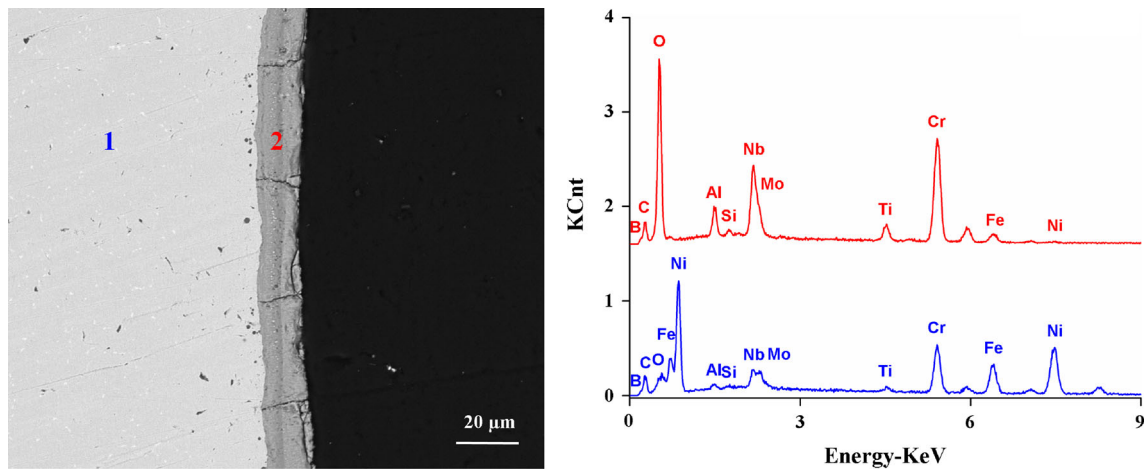


Fig. 10 Comparison of elemental composition between the bulk material (Area 1) and the recast layer (Area 2) of high-temperature alloy. Laser power 80 W; beam expanding ratio 4

Table 2 Comparison of elemental composition (wt%) between the bulk material and the recast layer of high-temperature alloy

Element	B	C	O	Al	Si	Nb	Mo	Ti	Cr	Fe	Ni
Bulk material 1	2.36	5.38	0.31	0.58	0.18	4.93	2.50	1.19	16.92	16.51	49.14
Recast layer 2	2.23	4.81	24.17	2.51	0.47	15.79	0.44	3.84	39.10	5.45	1.19

two parameters are examined, and a further research will be performed to investigate the influence of other factors, e.g., assist gas pressure, laser beam focal position, and trepan speed, on the hole quality (conicity, circularity, melting and spattering content, micro-crack, recast layer, etc.) in order to acquire a comprehensively optimized laser drilling parameters.

5 Conclusions

In the present study, a quantitative method for the characterization of hole quality during laser trepan drilling of high-temperature alloy was developed, from which the optimal drilling parameters including laser power and beam expanding ratio were gained according to the calculation of conicity and circularity of the holes. In addition, melting and spattering contents were observed at both the entrance end and the exit end, and micro-cracks and recast layer were detected along the side wall of the holes. The quantitative method developed in the present study may be applied in the characterization of hole quality in laser drilling and other drilling conditions.

Acknowledgments This study was supported by National Basic Research Program of China (Grant No. 2011CB013004), National Natural Science Foundation of China (Grant No. 51375008), Tsinghua University Initiative Scientific Research Program (Grant No.

20151080366), and the Research Fund of State Key Laboratory of Tribology, Tsinghua University, China (Grant No. SKLT2015B03).

References

- W. Schulz, U. Eppelt, R. Poprawe, Review on laser drilling I. Fundamentals, modeling, and simulation. *J. Laser Appl.* **25**, 012006 (2013)
- A. Ancona, D. Nodop, J. Limpert, S. Nolte, A. Tunnermann, Microdrilling of metals with an inexpensive and compact ultra-short-pulse fiber amplified microchip laser. *Appl. Phys. A* **94**, 19–24 (2009)
- R.S. Bunker, A review of shaped hole turbine film cooling technology. *J. Heat. Transf.* **127**, 441–453 (2005)
- X.D. Wang, A. Michalowski, D. Walter, S. Sommer, M. Kraus, J.S. Liu, F. Dausinger, Laser drilling of stainless steel with nanosecond double-pulse. *Opt. Laser Technol.* **41**, 148–153 (2009)
- J.K.M. Garofano, H.L. Marcus, M. Aindow, Nanoscale carbide precipitation in the recast layer of a percussion laser-drilled superalloy. *Scripta Mater.* **61**, 943–946 (2009)
- H.K. Sezer, L. Li, M. Schmidt, A.J. Pinkerton, B. Anderson, P. Williams, Effect of beam angle on HAZ, recast and oxide layer characteristics in laser drilling of TBC nickel superalloys. *Int. J. Mach. Tool Man.* **46**, 1972–1982 (2006)
- X.Y. Wang, G.K.L. Ng, Z. Liu, L. Li, L. Bradley, EPMA microanalysis of recast layers produced during laser drilling of type 305 stainless steel. *Thin Solid Films* **453–454**, 84–88 (2004)
- B. Kang, G.W. Kim, M.Y. Yang, S.H. Cho, J.W. Park, A study on the effect of ultrasonic vibration in nanosecond laser machining. *Opt. Laser Eng.* **50**, 1817–1822 (2012)
- J.A. Porter, Y.A. Louhisalmi, J.A. Karjalainen, S. Fuger, Cutting thin sheet metal with a water jet guided laser using various

- cutting distances, feed speeds and angles of incidence. *Int. J. Adv. Manuf. Technol.* **33**, 961–967 (2007)
10. J. Kaspar, A. Luft, S. Nolte, M. Will, E. Beyer, Laser helical drilling of silicon wafers with ns to fs pulses: scanning electron microscopy and transmission electron microscopy characterization of drilled through-holes. *J. Laser. Appl.* **18**, 85–92 (2006)
 11. K.H. Leitz, B. Redlingshofer, Y. Reg, A. Otto, M. Schmidt, Metal ablation with short and ultrashort laser pulses. *Phys. Proced.* **12**, 230–238 (2011)
 12. S. Juodkazis, H. Okuno, N. Kujime, S. Matsuo, H. Misawa, Hole drilling in stainless steel and silicon by femtosecond pulses at low pressure. *Appl. Phys. A* **79**, 1555–1559 (2004)
 13. H.Y. Zhang, J.K. Di, M. Zhou, Y. Yan, R. Wang, An investigation on the hole quality during picosecond laser helical drilling of stainless steel 304. *Appl. Phys. A* **119**, 745–752 (2015)
 14. H.Y. Zhang, J.K. Di, M. Zhou, Y. Yan, A comparison in laser precision drilling of stainless steel 304 with nanosecond and picosecond laser pulses. *Chin. J. Mech. Eng.* **27**, 972–977 (2014)
 15. S. Leigh, K. Sezer, L. Li, C. Grafton-Reed, M. Cuttall, Recast and oxide formation in laser-drilled acute holes in CMSX-4 nickel single-crystal superalloy. *Proc. IMechE Part B J. Eng. Manuf.* **224**, 1005–1016 (2009)
 16. V. González-Castro, J. Debayle, J.C. Pinoli, Color adaptive neighborhood mathematical morphology and its application to pixel-level classification. *Pattern Recogn. Lett.* **47**, 50–62 (2014)
 17. A. Barchanski, D. Funk, O. Wittich, C. Tegenkamp, B.N. Chichkov, C.L. Saji, Picosecond laser fabrication of functional gold-antibody nanoconjugates for biomedical applications. *J. Phys. Chem. C* **119**, 9524–9533 (2015)
 18. K.H. Leitz, H. Koch, A. Otto, M. Schmidt, Numerical simulation of process dynamics during laser beam drilling with short pulses. *Appl. Phys. A* **106**, 885–891 (2012)
 19. S. Bandyopadhyay, J.K. Sarin, Sundar, G. Sundararajan, S.V. Joshi, Geometrical features and metallurgical characteristics of Nd:YAG laser drilled holes in thick IN718 and Ti-6Al-4 V sheets. *J. Mater. Process. Technol.* **127**, 83–95 (2002)
 20. D.K.Y. Low, L. Li, A.G. Corfe, Characteristics of spatter formation under the effects of different laser parameters during laser drilling. *J. Mater. Process. Technol.* **118**, 179–186 (2001)
 21. W.T. Chien, S.C. Hou, Investigating the recast layer formed during the laser trepan drilling of Inconel 718 using the Taguchi method. *Int. J. Adv. Manuf. Technol.* **33**, 308–316 (2007)
 22. F. Dausinger, Femtosecond technology for precision manufacturing: fundamental and technical aspects. *RIKEN Rev.* **50**, 77–82 (2003)